Acta Materialia 120 (2016) 130–137

Contents lists available at ScienceDirect

Acta Materialia

journal homepage: www.elsevier.com/locate/actamat

Full length article

Dislocation induced strain glass in $Ti_{50}Ni_{45}Fe_5$ alloy

Jian Zhang, Dezhen Xue, Xiaoying Cai, Xiangdong Ding*, Xiaobing Ren, Jun Sun

State Key Laboratory for Mechanical Behavior of Materials, Xi'an Jiaotong University, Xi'an 710049, China

ARTICLE INFO

Article history:
Received 30 April 2016
Received in revised form
3 August 2016
Accepted 5 August 2016

Keywords:
Dislocations
Strain glass
Martensitic transformation
Phase diagram
Transmission electron microscopy

ABSTRACT

Short-range strain-ordered strain glass (STG) appears when the kinetic limitation (local stress field produced by random defects) is strong enough to suppress thermodynamic driven long-range strain-ordered martensitic transition. The point defects and precipitates have been proven to be effective to suppress the martensitic transition and trap the system in a frozen STG state. The dislocations can also introduce the random stress field down to atomic scale, however the effectiveness of which on the crossover from martensite to STG transition remains unknown. Here we report the first experimental finding of the dislocation induced STG transition in a $Ti_{50}Ni_{45}Fe_5$ martensitic alloy when the sample was cold compressed by over 20% plastically. Being different from the point defects and precipitates, the dislocations do not change the chemical composition of the matrix and consequently do not vary the transition temperature too much. Our finding verifies the effectiveness of local randomness on the crossover from martensite to STG transition and suggests that the global effect of defects is not a necessary condition for the occurrence of STG. The present finding may promote the application of STG alloy by assisting on the tuning of functional temperature range in STG alloy through adding the randomness of dislocations.

1. Introduction

Symmetry breaking at the martensitic transformation temperature produces two distinct strain states in ferroelastic/martensitic systems, a strain disordered high symmetry parent phase and a strain ordered low symmetry martensite [1,2]. The martensite is featured by a long-range strain ordering. After breaking such long-range strain ordering, a new stain state named strain glass (STG) is observed in a variety of martensitic alloys [2,3]. STG is a frozen state of local strain order, characterized by martensite nano-domains imbedded in a parent phase matrix, the dynamic freezing, and the breaking down of ergodicity [3,4]. This so-called "strain glass" is not only of theoretical interest as a new member of ferroic glasses; it also possesses a number of interesting properties such as shape memory effect and superelasticity [5–7], originating from a new mechanism based on the stress-induced STG into martensite transition.

Experimentally, there are several ways to break long-range stain ordering to form the STG. Point defects have been known to produce local random stress field to induce STG. A variety of point defect induced STG systems were found, including Ni-rich Ti-Ni [8], Ti-Ni-X (X = Fe, Co, Cr, Mn) [9–11], Ti-Pd-X (X = Fe, Co, Cr, Mn) systems [12], Au-Cu-Al [13] as well as ferroelectric [14] and ferromagnetic systems [15,16]. Notably, the formation of STG is not merely restricted to the doping of point defects. It can be induced by introducing nano-size coherent precipitates [17,18] as well, since these precipitates generate random local stress field [19] to suppress the long range strain ordering. To summarize, all stain glass transitions found so far falls into the two categories, i.e. point defect induced STG and precipitate induced STG as schematically shown in Fig. 1a and b.

The underlying mechanism for the formation of STG is widely investigated by various theoretical works. Phase field modeling shows that either the point defects or the precipitates introduce two effects to the martensitic system [20]: 1) A global effect, which alters the global thermodynamic stability of martensite, and namely lowers the transformation temperature of the whole sample. For example, point defects or precipitates change the composition of the matrix, and thus alter the global thermodynamic stability of martensite [21]; 2) A local effect, which creates local distortions or local random stress field. The local random field varies the local transition temperatures. Thus the latter local effect is also somewhat similar to the local transition temperature fluctuation effect, i.e., spatial fluctuation of transition temperature [20].

* Corresponding author.
E-mail address: dingxd@mail.xjtu.edu.cn (X. Ding).

http://dx.doi.org/10.1016/j.actamat.2016.08.015
1359-6454/

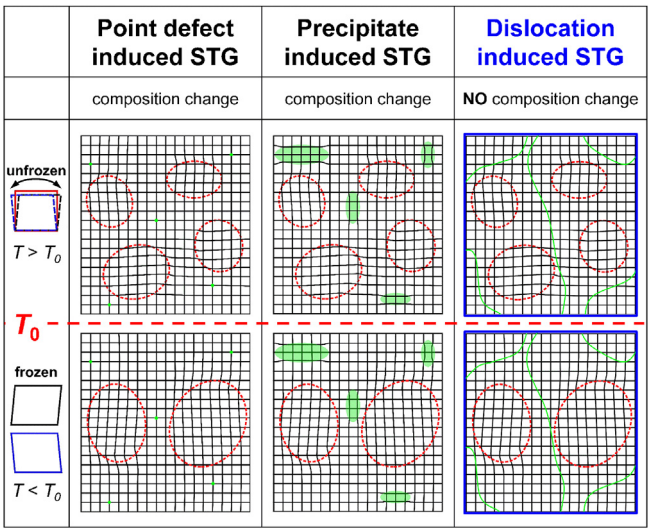

Fig. 1. Schematic microscopic pictures of the strain freezing process in STG induced by point defects, precipitates and dislocations.

Recent a renormalization group analysis based on a martensitic pseudospin model showed that quenched disorder (i.e., local effect, either local random field or randomness in the transition temperature) itself could result in the STG [20,22], especially in the situation where the global effect is weak or even absent [22]. However, experimentally the introduction of either point defects or precipitates not only produces local random field (local effect), but also involves a composition change, which simultaneously varies the transformation temperature of the system (global effect). Therefore, it is still unclear in experiment whether the global effect is a necessary condition for the formation of STG. One critical circumstance to answer this question is to generate STG via only enhancing the local effect but not involving the change of global effect. This requires a new way, instead of either doping point defects or precipitation, to suppress the martensitic transition by producing random local stress field, but does not vary the transition temperature of the system.

To this end, the dislocations are the most promising candidate, since the introduction of random dislocations produces the random stress field down to atomic scale as illustrated in Fig. 1c, but does not affect the chemical composition of the matrix [23]. Thus if dislocation can induce STG, it is a critical result to answer the question whether global effect is a necessary condition for the occurrence of STG. In the present study, we report the first finding of the dislocation induced STG transition in a $Ti_{50}Ni_{45}Fe_5$ martensitic alloy where the high density random dislocations are introduced through cold compression by over 20% thickness reduction.

2. Experimental procedures

$Ti_{50}Ni_{45}Fe_5$ alloy, which is at the boundary of crossover composition regime [24] from R-martensite to STG, is selected to demonstrate the effectiveness of dislocations on the STG formability. Another advantage of utilizing $Ti_{50}Ni_{45}Fe_5$ alloy is to avoid the stress induced R-phase and/or B19′ martensitic transitions during compression, which certainly will affect the dislocation substructure [25] and reduce the randomness of the dislocations. The alloy with nominal composition $Ti_{50}Ni_{45}Fe_5$ was prepared by induction melting and casting with a mixture of 99.9% pure Ti, 99.9% pure Ni and 99.9% pure Fe in the flow of argon gas. As Ti is highly active metal, CaO crucibles instead of graphite ones were employed in order to avoid the reaction between container and Ti during the induction melting at high temperatures. The obtained cast ingot was spark cut into sheet specimens and solution-treated at 1000 °C for 1 h before the subsequent experiments.

In order to elucidate the effect of dislocation on the STG formability, various densities of dislocation were introduced through compression at room temperature, by controlling the amounts of thickness reduction ($\varepsilon = (t_0 - t)/t_0$, where the t_0 and t are the thicknesses before and after compression). The compression was carried out in a SHIMADZU hydrostatic compressor with maximum load of 20 ton. In this paper, four sets of specimens were studied with different thickness reductions: 1) as solution-treated state, i.e. $\varepsilon = 0\%$; 2) $\varepsilon = 10.5\%$; 3) $\varepsilon = 22.6\%$; and 4) $\varepsilon = 31.2\%$.

The thermal effect and dynamical mechanical properties of the transitions (R martensite transition and STG transition) in four sets of specimens were investigated by differential scanning calorimetry(DSC) and dynamical mechanical analysis (DMA). DSC test was performed in TA Q200 DSC with a heating/cooling rate of 10 K/min. The dynamical mechanical properties were conducted on a TA Q800 DMA using step cooling method with single cantilever mode. The internal friction and storage modulus were recorded at five frequencies (0.2/0.4/1/4/10 Hz) as a function of temperature.

The X-ray diffraction (XRD) line profiles of samples ($\varepsilon = 22.6\%$ and 31.2%) were collected at 298 K and 113 K by using Rigaku 2000 XRD equipped with a heating/cooling stage. In addition, transmission electron microscopy (TEM) observation was performed on the sample with $\varepsilon = 22.6\%$ at 298 K, 203 K, 153 K and 113 K with Phillips CM20 TEM, equipped with a Gatan 636HD heating/cooling holder. An FEI Tecnai F20G2 with a HAADF (high angle annular dark field) detector was used to study the dislocation substructure and density of the specimens subjected to 10.5%, 22.6% and 31.2% thickness reduction. The TEM specimens were mechanically polished, and then punched into discs with diameter 3 mm. Finally, the small discs were electro-polished using a twin-jet apparatus operating at 260 K. The electrolytic solution consisted of 10 vol% $HClO_4$ and 90 vol% CH_3CH_2OH.

3. Experimental results

In Fig. 2, the TEM micrographs (STEM-HAADF mode) taken from $[111]_{B2}$ zone axis show the dislocation substructures, formed as a result of the plastic compression. The dislocations in the sample of $\varepsilon = 10.5\%$ possess a cellular structure, and become denser and random with the increase of thickness reduction from 22.6% to 31.2% as shown in Fig. 2. To reveal the transition characteristics, the DSC and DMA measurements were performed.

In Fig. 3, the DSC charts of four sets of $Ti_{50}Ni_{45}Fe_5$ samples ($\varepsilon = 0\%$, 10.5%, 22.6% and 31.2%) are presented in a stack fashion with a normalized scale. Both the exothermic peak during cooling (Fig. 3a) and endothermic peak during heating (Fig. 3b) are broadened and lowered with the increase of thickness reduction. For the $Ti_{50}Ni_{45}Fe_5$ sample with $\varepsilon = 0\%$, the DSC peaks are very sharp. The latent heat and hysteresis are measured to be 160 J/mol and 10 K respectively, which are consistent with the values in the literature [26]. These sharp peaks hence denote one-step B2 to R martensite transition. When the sample is compressed 10.5% plastically, the DSC peaks are much lowered. And the DSC peaks are further smeared out and replaced by very broad and weak humps when the thickness reduction reaches 22.6%. Such a transaction from peaks to humps has been also found in various systems [10–12], accompanying the crossover from normal martensite to STG transition. In order to show the difference between the DSC peaks and humps, the first derivatives of the cooling parts of DSC curves in Fig. 3a have been calculated and presented in Fig. 4. It can

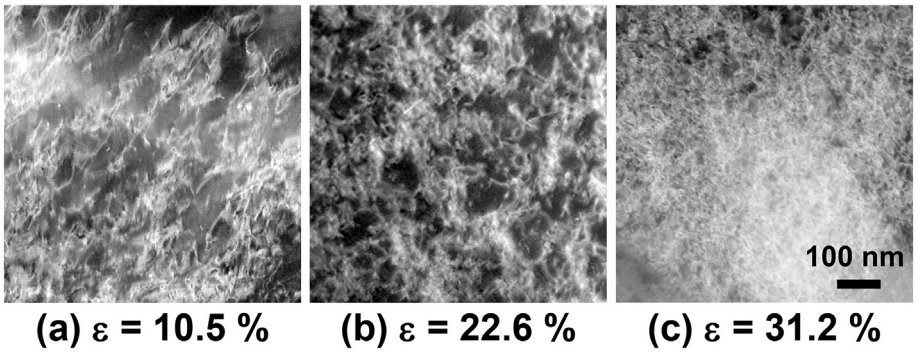

Fig. 2. STEM-HAADF images of $Ti_{50}Ni_{45}Fe_5$ samples with thickness reductions of $\varepsilon = 10.5\%$ (a), 22.6% (b) and 31.2% (c). The micrographs were taken along the $[111]_{B2}$ zone axis at 298 K.

be seen clearly that there are dips/peaks in first derivative curves of the samples with $\varepsilon = 0\%$ and 10.5%, while no such feature for those with higher thickness reduction. It indicates that the transition in the sample of $\varepsilon = 10.5\%$ is still B2 to R-phase martensitic transition, while the transition in the samples of $\varepsilon = 22.6\%$ and 31.2% is not. It will be further verified to be STG transition by DMA results presented below.

Fig. 5 displays the temperature dependence of internal friction (Fig. 5a) and storage modulus (Fig. 5b) curves for non-deformed and deformed $Ti_{50}Ni_{45}Fe_5$ samples measured at various frequencies by DMA. The DMA curves for the samples with $\varepsilon = 0\%$ and 10.5% shows frequency independent feature, as a clear evidence of a martensitic transition. Moreover, R_s temperatures determined by DSC curves during cooling (Figs. 3a and 4) are consistent with the starting temperatures of the storage modulus dips for both samples with $\varepsilon = 0\%$ and 10.5% as indicated by the arrows in Fig. 5b.

When the thickness reduction further increases, the DMA curves show a different behavior. Both temperatures of the storage modulus dips and internal friction peaks of the samples with $\varepsilon = 22.6\%$ and 31.2% show strong frequency dispersion, which means that the dip and peak temperatures are frequency dependent. It is worth mentioning that both magnitudes of storage modulus dips and internal friction peaks gradually decrease with the increase of the thickness reduction. Such phenomena are very similar to the case of the point defect and precipitate induced STGs.

For the clarity, the DMA curves of $\varepsilon = 22.6\%$ and 31.2% samples are again presented in Fig. 6 with a smaller scale. The dip temperatures T_g of the storage modulus (Fig. 6b) exhibits a frequency

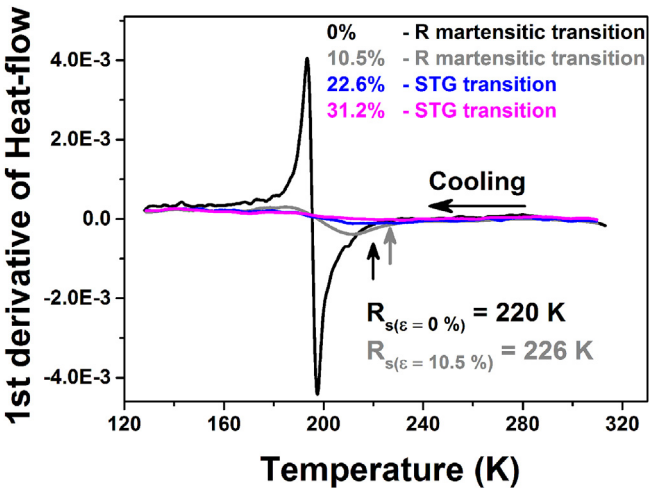

Fig. 4. 1st derivatives of heat-flow in the cooling parts of the DSC charts shown in Fig. 3a.

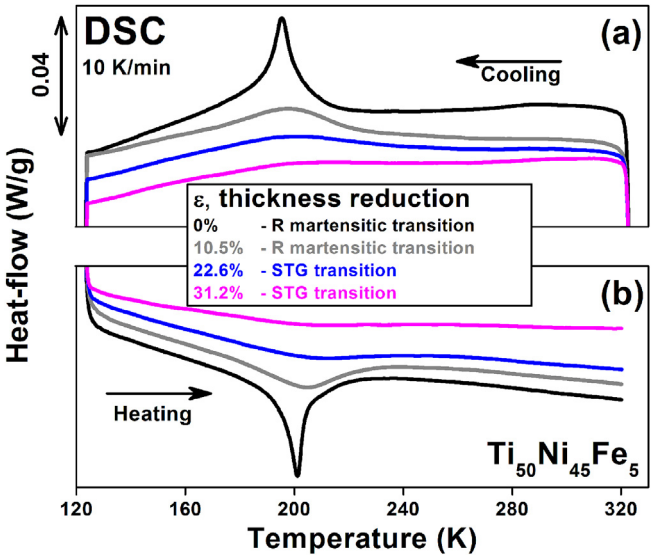

Fig. 3. DSC charts of $Ti_{50}Ni_{45}Fe_5$ with various thickness reductions ($\varepsilon = 0\%$, 10.5%, 22.6% and 31.2%), recorded during (a) cooling, and (b) heating.

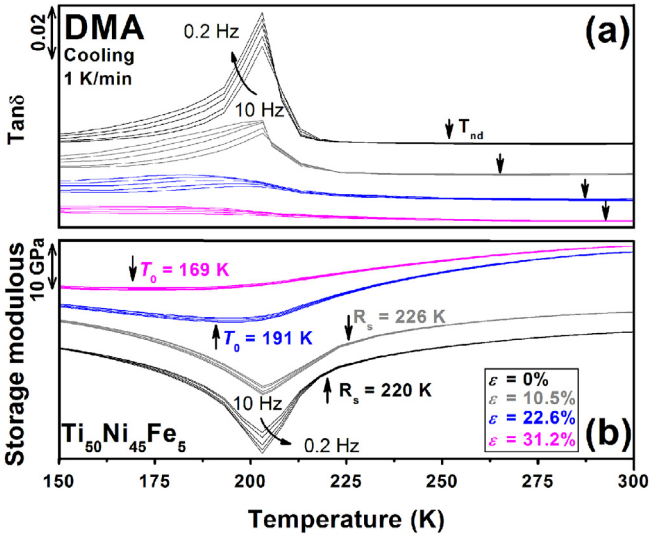

Fig. 5. (a) Storage modulus and (b) internal friction (tanδ) curves of $Ti_{50}Ni_{45}Fe_5$ samples with various thickness reductions ($\varepsilon = 0\%$, 10.5%, 22.6% and 31.2%).

dependence. As shown in the insets of Fig. 6, it follows the Vogel–Fulcher relaxation ($\omega = \omega_0 exp[-E_a/k(T_g - T_0)]$, where T_0 is the ideal frozen temperature of STG transition). It is deferent from the normal Debye relaxation [27,28]. Such a behavior is a characteristic of STG transition [11]. According to the Vogel-Fulcher fitting, the T_0 for 22.6% and 31.2% deformed $Ti_{50}Ni_{45}Fe_5$ are 179 K and 154 K, respectively. Therefore, the introduction of dislocations over certain critical density results in a crossover from martensite to STG transition. Besides, another important temperature T_{nd} (the starting temperature of the appearance of precursory nano-domains) increases with the increase of thickness reduction as indicated in Fig. 5a. It is determined by the temperature at which the internal friction starts to increase [11]. Note that T_{nd} is well above the R_s or T_0. This temperature corresponds to the Burns temperature in relaxor ferroelectrics [29].

To further confirm that the severely deformed $Ti_{50}Ni_{45}Fe_5$ alloy undergoes a STG transition and reveal the evolution of the microscopic structure during such STG transition, the in-situ cooling XRD and TEM were performed and presented below.

In-situ XRD measurements were performed in $Ti_{50}Ni_{45}Fe_5$ with $\varepsilon = 22.6\%$ and 31.2% and presented in Fig. 7. The XRD line profiles in Fig. 7 show that the 110_{B2} peaks remain singlet when the temperature was cooled from 298 K to 113 K. It confirms that the B2 → R martensitic transition has been suppressed in both cases.

In-situ cooling TEM observation was performed for a 22.6% deformed sample at $T > T_0$ (298 K), $T \sim T_0$ (203 K), and $T < T_0$ (153 K and 113 K), respectively. Through in-situ TEM observations, the microstructure evolution of 22.6% deformed $Ti_{50}Ni_{45}Fe_5$ was monitored when the TEM foil was cooled spanning T_0, as presented in Fig. 8. The faint diffuse streaks along three <110>$_{B2}$ directions in the diffraction patterns indicate the formation of R-like nano-domains during cooling [24].

To summarize, the $Ti_{50}Ni_{45}Fe_5$ undergoes normal R martensitic transition even when it is plastically deformed for 10.5%; while the martensitic transition will be fully suppressed and STG transition occurs when the thickness reduction reaches $\varepsilon = 22.6\%$. Such crossover from martensite into STG transition is solely due to the high density random dislocations (Fig. 2b and c) introduced by plastic compression. Therefore, the STG found in the present study is termed dislocation induced STG. Besides, the nano-domains of the dislocation induced STG in $Ti_{50}Ni_{45}Fe_5$ are also found to possess R-like local symmetry, which is the same as those in point defect and precipitate induced STGs in Ti-Ni-based and Ti-Pd-based systems [5,11,12,30].

4. Discussions

4.1. Phase diagram of $Ti_{50}Ni_{45}Fe_5$ with respect to dislocation density

The above systematic experimental results demonstrate how the transition features (e.g. T_{nd}, R_s and T_0) of $Ti_{50}Ni_{45}Fe_5$ gradually change with the increase of thickness reduction. To better understand the physical nature of such changes, a phase diagram will be built with respect to dislocation density since the change of transition features are due to the random dislocations introduced by thickness reduction.

The mean dislocation densities ρ are measured from the STEM-HAADF images in Fig. 2 by using the method described in Ref. [25], and are plotted against the thickness reduction as shown in Fig. 9. ρ of the sample with $\varepsilon = 22.6\%$ is counted to be 564 μm^{-2}, which is hence defined as ρ_c for the dislocation induced crossover from martensite to STG transition as indicated in Fig. 9. In addition, the free spacing among the dislocation network ($Spacing_{dislo}$) is also presented alongside, which is calculated through the equation of $Spacing_{dislo} = 2 \times (\pi\rho_{dislo})^{-1/2}$ [23,25]. Clearly, dislocation density increases with the increase of the thickness reduction, which corresponds to a decrease of $Spacing_{dislo}$.

Spacing among the defects can significantly affect the phase transformation behaviors. Previous works [31,32] show that the spacing among precipitates play a crucial rule in the occurrence of multistage martensitic transformations in aged Ni-rich Ti-Ni. Here,

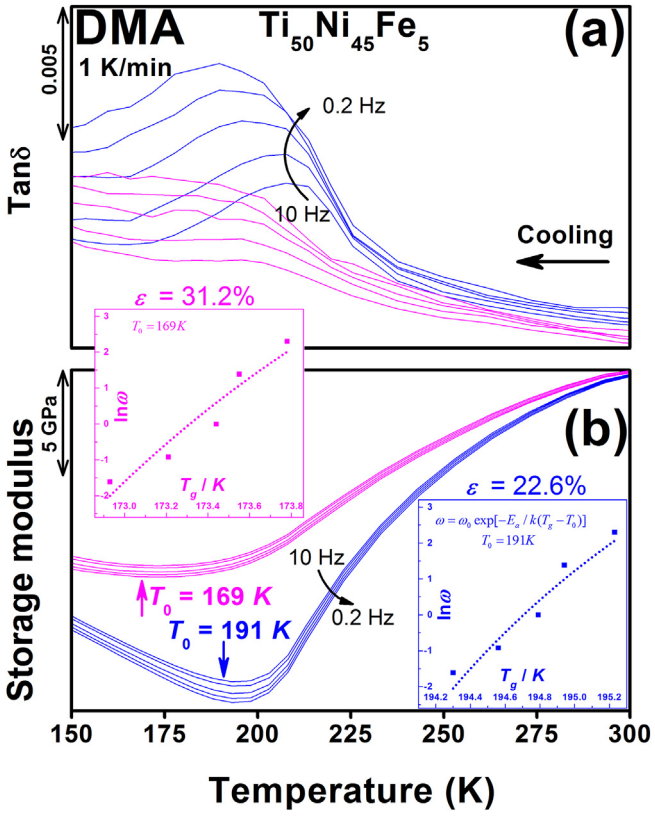

Fig. 6. (a) Storage modulus and (b) internal friction (tanδ) curves of $Ti_{50}Ni_{45}Fe_5$ samples with $\varepsilon = 22.6\%$ and 31.2% during cooling. The insets show the results of Vogel-Fulcher fitting of T_g (the dip temperatures of storage modulus curves in (b)) and the ideal frozen temperatures (T_0).

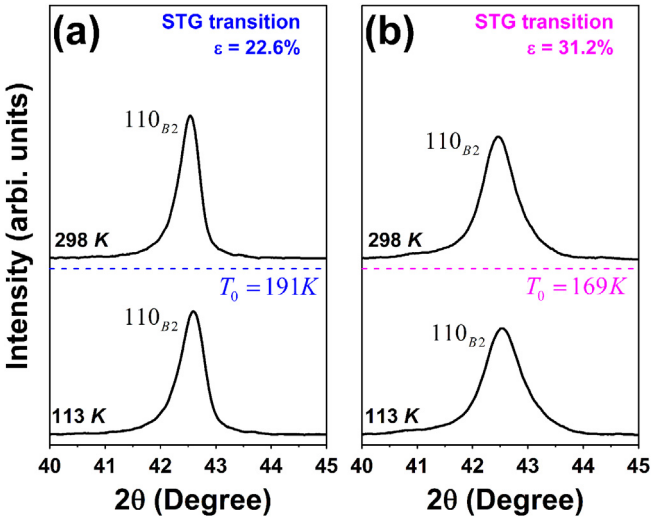

Fig. 7. XRD line profiles at 298 K and 113 K for plastically deformed $Ti_{50}Ni_{45}Fe_5$ samples with $\varepsilon = 22.6\%$ and 31.2%.

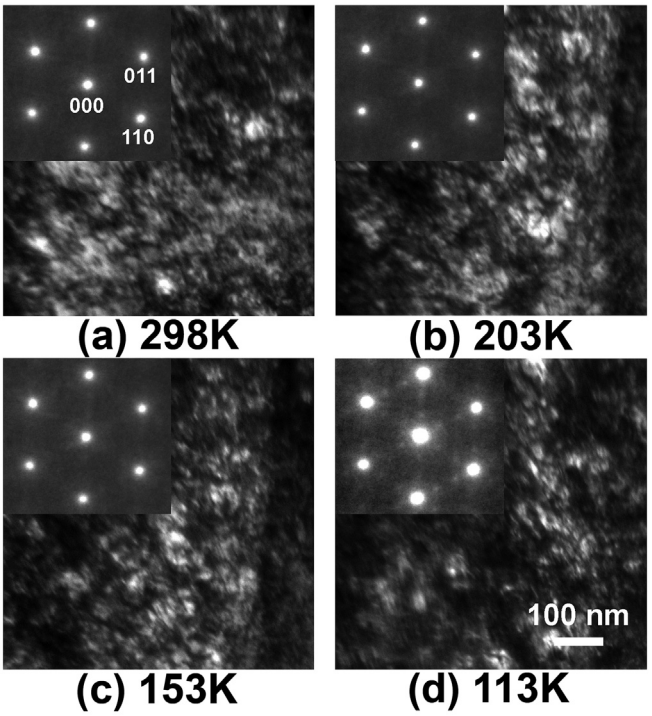

Fig. 8. Bright-field images during in-situ cooling of $Ti_{50}Ni_{45}Fe_5$ sample with $\varepsilon = 22.6\%$. (a) 298 K ($T > T_g$); (b) at 203 K ($T \sim T_g$); (c) and (d) at 153 K and 113 K ($T < T_g$). The zone axis is $[111]_{B2}$. The insets are the corresponding diffraction patterns.

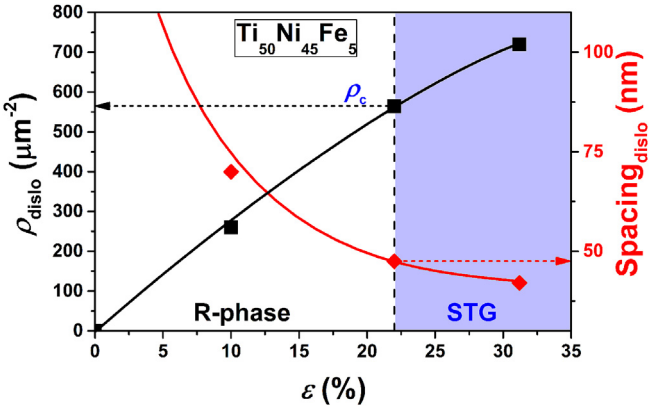

Fig. 9. Increase of the mean dislocation density ρ (left Y-axis) and decrease of the average $Spacing_{dislo}$ (right Y-axis) with the increase of thickness reduction in $Ti_{50}Ni_{45}Fe_5$. ρ_c ($= 564\ \mu m^{-2}$), defined as the $Spacing_{dislo}$ decreases down to 48 nm ($\varepsilon = 22.6\%$ in $Ti_{50}Ni_{45}Fe_5$), indicates the critical dislocation density that induces the crossover from R martensite to STG transition.

the decrease of $Spacing_{dislo}$ leads to the crossover from R martensite to STG transition, since the maximum size of the R-like nano-domains or R martensite is limited by $Spacing_{dislo}$ among the dislocation network. For the dislocation induced STG, the corresponding $Spacing_{dislo}$ of ρ_c ($= 564\ \mu m^{-2}$) is 48 nm, which implies that the maximum size of R-like nano-domain is below 48 nm even down to 0 K. It is quite close to 50 nm, the detection limit of a lab XRD (R-like nano-domains of the size above 50 nm can be detected as R martensite, evident with the splitting of certain peaks (such as 110_{B2}) in XRD line profile) [24].

It is interesting to note that such a huge dislocation density ($\rho_c = 564\ \mu m^{-2}$) has to be reached in order to fully suppress the R martensite into STG transition, even though the current $Ti_{50}Ni_{45}Fe_5$ matrix bears quite a lot point defects (5 at.% Fe). It hence suggests that the dislocations suppress the R martensite transition into STG transition through a kinetic origin by limiting the scale of R-like nano-domain growth. Thus, ρ_c ($564\ \mu m^{-2}$, or namely $Spacing_{dislo} = 48$ nm) might be a universal value for dislocation induced crossover from R martensite into STG in all ferroelastic/martensitic systems with R thermodynamic instability disregarding the composition of matrix.

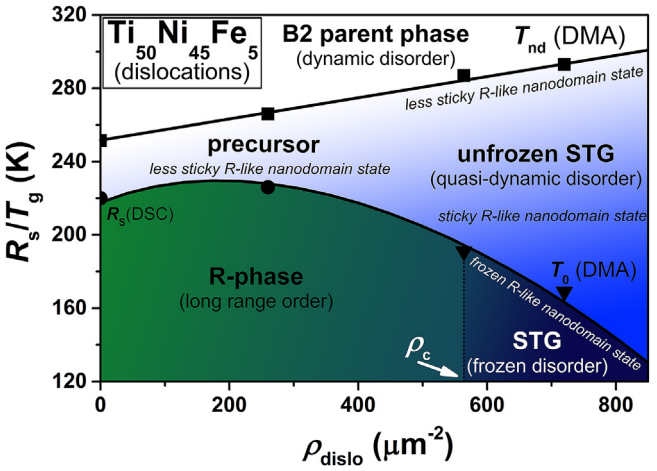

Fig. 10. Transition-temperature vs dislocation-density phase diagram of $Ti_{50}Ni_{45}Fe_5$, which undergoes R martensite transition with $\rho < \rho_c$ and STG transition with $\rho \geq \rho_c$. $\boldsymbol{T_{nd}}$ (■) is the starting temperature of the appearance of quasi-dynamic R-like nano-domain, which is the temperature at which internal friction starts to increase from DMA measurements (Fig. 5a); R-phase transition starting temperatures $\boldsymbol{R_s}$ (●) are determined by DSC results (Figs. 3 and 4). The ideal frozen temperature of STG transition $\boldsymbol{T_0}$ (▼) is obtained from storage modulus curves of DMA measurements (Fig. 6).

Based on the dislocation densities and transition characteristic temperatures, a phase diagram for $Ti_{50}Ni_{45}Fe_5$ ferroelastic system with respect to the dislocation density ρ is built up and presented in Fig. 10. The new phase diagram seems quite similar to those of point defect induced STG [9–11], but the physical nature is different. The new phase diagram reveals a key phenomenon: dislocations cause the crossover from martensite to STG transition as the dislocation-density reaches a critical value ρ_c.

4.2. Physical nature of the dislocation induced crossover from martensite to STG

In this section, the physical nature of the dislocation induced crossover from martensite to STG will be provided based on a unified effect of dislocation on the R-phase (B2 → R martensite of domain size over 50 nm) as well as STG transition (B2 → frozen STG state with R-like nano-domains of size less than 50 nm).

In order to unifying the effect of dislocation on both R martensite and STG transitions, the R martensite transition is divided into three stages based on the transition kinetics: **1st stage** ($T = T_{nd}$): nucleation of quasidynamic R-like nano-domains; **2nd stage** (R_s (or T_0) $< T < T_{nd}$): initial growth of R-like nano-domains within the size of 50 nm; **3rd stage** ($T \leq R_s$): the formation of R martensite with domain size over 50 nm. Under such a scheme, the STG transition can be treated as a "non-complete R martensite transition" only involving the first two stages: after the nucleation of R-like nano-domains below T_{nd}, the system is frozen into STG state with nano-domains size <50 nm at T_0. In the following, we propose a physical picture on the dislocation induced crossover from martensite to STG transition, as shown in Fig. 11.

1) Dislocation-free system ($\rho = 0$): R martensite transition

The physical picture for the R martensite transition in a dislocation-free system is shown in Fig. 11B (a1) to (a4). It is important to note that dislocation-free system is not necessary to be defect-free. For generality, the current discussion is based on a point defect containing ferroelastic system (i.e. $Ti_{50}Ni_{45}Fe_5$ in the present study).

At $T > T_{nd}$ (Fig. 11B(a1)), thermal fluctuation is strong and can overcome the defect-induced (only point defects) local stress; hence the system still stays in a dynamically disordered state (i.e., a normal parent phase) in despite of the random stresses.

Upon cooling to $T < T_{nd}$, thermal fluctuation becomes weaker and cannot overcome some of the defect-induced local stresses. As a result, a random distribution of a small amount of quasidynamic R-like nanodomains, as shown in Fig. 11B(a2). This quasidynamically disordered strain state below T_{nd} corresponds to the experimentally observed precursor state shown in Fig. 10.

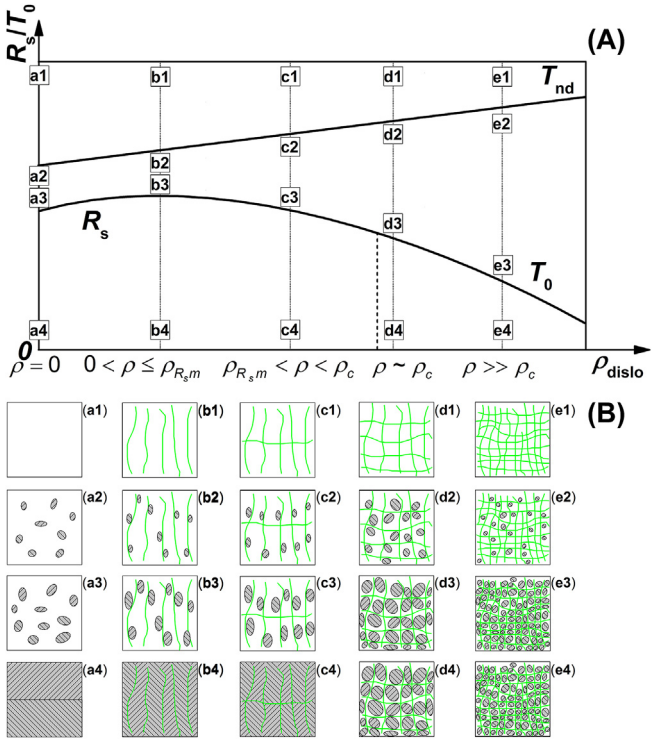

Fig. 11. (A) A simplified phase diagram of Fig. 10, where the temperature of each microscopic picture is indicated. (B) Microscopic pictures about the crossover behavior from normal R martensite to dislocation induced STG as a function of dislocation density in $Ti_{50}Ni_{45}Fe_5$. The dislocations are illustrated as green curved lines, while the R-phase or R-like nano-domains are represented in color grey and filled with oblique lines. (a1), (a2), (a3), and (a4) show the transition process of dislocation-free martensitic system ($\rho = 0$): from dynamically disordered state (a1) to quasidynamically disordered state ((a2) and (a3)), then to long-range ordered R-phase state (a4). (b1), (b2), (b3), and (b4) show the transition process of slightly defected (dislocation) martensitic system ($0 < \rho < \rho_{Rsm}$, ρ_{Rsm} stands for the dislocation density where has the maximum R_s): from dynamically disordered state (b1) to quasidynamically disordered state ((b2) and (b3)), finally to long-range ordered state R-phase (b4). (c1), (c2), (c3), and (c4) show the transition process of martensitic system with relatively high dislocation density ($\rho_{Rsm} < \rho < \rho_c$): from dynamically disordered state (c1) to quasidynamically disordered state ((c2) and (c3)), finally to long-range ordered state R-phase (c4). (d1), (d2), (d3), and (d4) show the freezing process of system with high-defect concentration ($\rho \sim \rho_c$) from a dynamically disordered state (d1) to quasidynamically disordered state ((d2) and (d3)), finally to frozen disordered state (d4). (e1), (e2), (e3), and (e4) show the freezing process of system with extremely large dislocation density ($\rho \gg \rho_c$): from a dynamically disordered state (e1) to quasidynamically disordered state ((e2) and (e3)), finally to frozen disordered state (e4). (For interpretation of the references to color in this figure legend, the reader is referred to the web version of this article.)

With the temperature approaching R_s, the quasidynamic R-like nanodomains becomes denser and bigger (still smaller than 50 nm in size) (Fig. 11B(a3)) due to the lowering of thermal kinetic energy (k_BT).

As the temperature further decreases to $T < R_s$, the quasidynamically disordered strains undergo a long-range strain ordering, i.e., formation of R martensite, as a consequence of the thermodynamic instability of the parent phase.

2) Low dislocation density system ($0 < \rho < \rho_c$): weak R martensite transition

The previous works proved that the dislocations promoted the nucleation of R-phase (namely formation of precursory R-like nanodomains) manifested by the rising of T_{nd}. However, the R_s initially arises and then decreases as the dislocation network become denser (Fig. 10), which exhibits a maximum value at certain dislocation density defined as ρ_{Rsm} (Fig. 11). It can be understood by considering the two-fold effects of dislocation on the growth of R-like nano-domains into R martensite (i.e. R_s): 1) the dislocation promotes the growth of R-like nanodomains following its stress field; 2) while the dislocation retards or even prevents the growth of R-like nanodomains opposing to its stress field. Therefore, the initial increase of R_s since the former effect is dominant when the dislocation density is low ($<\rho_{R_sm}$) as illustrated in Fig. 11B (b1) to (b4); while the latter effect becomes dominate when the dislocations become dense ($>\rho_{R_sm}$) (Fig. 11B (c1) to (c4)), and hence R_s decreases. Despite of the changing of R_s, the transition phenomena are quite similar to that of dislocation-free case.

3) High dislocation density system ($\rho \sim \rho_c$): STG transition

Within this dislocation density range, dislocation promotes 1st and 2nd stages but fully suppresses the 3rd stage of the R martensite transition: T_{nd} increases and STG appears instead of R martensite.

T_{nd} is further increased (Fig. 11B(d1) to (d2)), and quasidynamic R-like nanodomains appear at even higher temperature and are denser as in Fig. 11B(d2).

As the temperature lowering, the increasing thermodynamic driving force towards R martensite assists the further growth of the nanodomains (Fig. 11B(d3)). However, the size of nanodomains can never reaches the critical size of 50 nm (Fig. 11B(d4)), the system is frozen into STG state at T_0. Upon further cooling ($T < T_0$), the growth of nanodomains is nearly stopped since the kinetic energy is very low as compared with the local barrier caused by dislocations [24].

4) Extremely high dislocation density system ($\rho \gg \rho_c$): STG transition

With extremely high dislocation density, dislocation promotes only 1st stage, slows 2nd stage and fully suppresses the 3rd stage of the transition: T_{nd} increases and T_0 decreases.

T_{nd} is further increased (Fig. 11B(e1) to (e2)), and quasidynamic R-like nanodomains appear at very high temperature and are very dense in numbers upon cooling to $T < T_{nd}$. The nanodomains experience the hindrance immediately after the nucleation. The growth of nanodomains become extremely difficult. Even when the temperature is close to the T_0 (Fig. 11B(e3)), the size of nanodomains is still quite small due to the restriction of free-spacing among the dislocation network (see Fig. 9). Upon further cooling ($T < T_0$), the growth of nanodomains is stopped (Fig. 11B(d4)) since the local barrier caused by dislocations is very high, although the thermodynamic driving force towards R martensite is increasing with cooling. Note that the T_0 also decreases for $\rho \gg \rho_c$, which is

quite similar to the point defect induced STG.

4.3. Comparison among point defect, precipitate and dislocation induced crossover from martensite into STG transition in ferroelastic/martensitic systems

As compared with the early versions of the phase diagrams [9–11,18], the new phase diagram with respect to the dislocation density (Fig. 10) shows several important new features as listed below.

1) T_{nd} increases linearly with the increase of dislocation density.

In contrast, in the Ti-Ni-Fe ternary STG system, T_{nd} decreases firstly and then begins to increase slowly as the point defects (Fe) content is high. As pointed out in Ref. [11], T_{nd} is dependent on both global effect and local effect of defects. As Fe point defects destabilize the R-phase by causing the decrease of R_s, the global effect of Fe leads to the decrease of T_{nd}. On the other hand, the local effect of defects always leads to the increase of T_{nd}. The initial decrease and then increase of T_{nd} with Fe content can be easily understood since the global effect is dominant at low Fe content while the local effect becomes dominant at high Fe content. Under this scheme, the linear increase of T_{nd} with increase of dislocation density approves that the random dislocations has no global effect but solely local effect on the R martensite transition. Similarly, the monotonic (not linear) increase of T_{nd} with Ni content (excessive Ni act as point defects) in binary Ti-Ni STG can also be explained as the global effect of Ni on R martensite transition is much less than that of Fe.

2) Transition temperature decrease due to the dislocation induced crossover from martensite into STG transition is very small.

Transition temperature decrease ($\Delta T(x_c)$) is defined as the difference between the martensitic transition temperature of defect-free system ($M_s(0)$) and STG transition temperature of system with critical defect concentration ($T_0(x_c)$), i.e. $\Delta T(x_c) = M_s(0) - T_0(x_c)$. It reflects the effectiveness of certain defects on inducing the crossover from martensite into STG transition. It is important since it determines the functional temperature range of STG alloy.

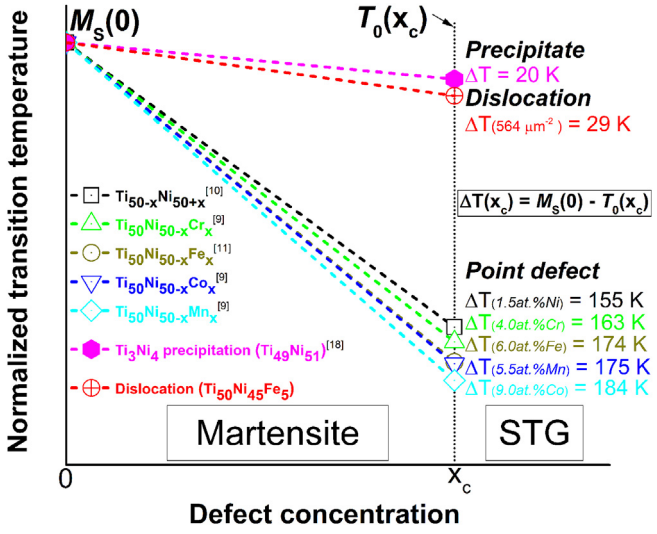

Fig. 12. Comparison of the transition temperature decreases (i.e. $\Delta T(x_c) = M_s(0) - T_0(x_c)$) due to defect (point defect, precipitate and dislocation) induced crossover from martensite into STG in the Ti-Ni-based ferroelastic/martensitic systems. For clarity, the $M_s(0)$ is normalized to the same value.

In Fig. 12, $\Delta T(x_c)$ of various kinds of defects are plotted. In general, the $\Delta T(x_c)$ of point defects are quite large (>150 K). As a result, the functional temperatures of point defect induced Ti-Ni-based STG alloys are much lower than room temperature, which might be one of the obstacles of their actual applications. In contrast, $\Delta T(x_c)$ of dislocation is very small (~29 K). The large difference of $\Delta T(x_c)$ of point defects and dislocations lies on the fact that the point defects have both global effect and local effect on the martensite transition, while dislocations only have local effect. However, for the case of precipitates (Ti_3Ni_4), the $\Delta T(x_c)$ is even smaller than that of dislocations. It is due to the opposite global effect of Ti_3Ni_4 precipitation (i.e. depletion of Ni in the matrix leads to the increase of R_s). Hence the dislocations and precipitates can better maintain the functional temperature of STG alloys.

3) There exists a critical dislocation density ($\rho_c = 564\ \mu m^{-2}$) for inducing the crossover from martensite into STG transition.

As the dislocations have only the local effect on the martensitic transition, ρ_c (564 μm^{-2}) might be a universal value for inducing the crossover from martensite into STG transition in all ferroelastic/martensitic systems with R thermodynamic instability disregarding the composition of matrix, since it is corresponding to the condition with $Spacing_{dislo} = 48$ nm where the occurrence of R martensite transition is fully suppressed through restricting the size of R-like nano-domains (<50 nm).

In contrast, the critical concentration of point defect for inducing STG is varying with respect to the type of doping element (seen in Fig. 12), which is simply due to the different global effect of different doping elements [21]. Besides, the critical density of precipitates is hard to determine since not only density but also the size and the coherency are essential for the local stress field around precipitates.

5. Conclusions

By means of cold compression, the random dislocations with various densities are successfully introduced into a $Ti_{50}Ni_{45}Fe_5$ ferroelastic/martensite system. After systematic investigations, we report in this paper the first set of experimental evidences of the dislocation induced STG transition in a $Ti_{50}Ni_{45}Fe_5$ when the sample was compressed by over 20% plastically. A critical dislocation density ρ_c (564 μm^{-2}, which equilibrates to $Spacing_{dislo} = 48$ nm) is identified and might be a universal value for inducing the crossover from martensite into STG transition in all ferroelastic/martensitic systems with R thermodynamic instability disregarding the composition of matrix. Based on the experimental results, a new phase diagram of $Ti_{50}Ni_{45}Fe_5$ with respect to dislocation densities is provided, where the crossover from martensite to STG transition is clearly presented and further explained by unitizing the virtue microscopic pictures. Furthermore, our finding verifies the effectiveness of short range disordering on the crossover from martensite to STG transition and suggests that the global effect is not a necessary condition for the occurrence of STG. Moreover, the comparisons of defect (point defect, precipitate and dislocation) induced crossover from martensite into STG transition suggest that the current finding may promoting the application of STG alloys by assisting on the fine tuning of the functionalities in STG alloy through adding another randomness of dislocations.

Acknowledgements

This work was supported by the National Science Foundation of China (51501145, 51320105014, 51321003), the 973 Programs of China (2014CB644003, 2012CB619401), the China Postdoctoral

Science Foundation (2015M570829), the Fundamental Research Funds for the Central Universities and the International Joint Laboratory for Micro/Nano Manufacturing and Measurement Technologies.

References

[1] E.K.H. Salje, Phase Transitions in Ferroelastic and Co-elastic Crystals, Cambridge University Press, Cambridge, England, 1990.

[2] K. Otsuka, C. Wayman, Shape Memory Materials, Cambridge University Press, Cambridge, 1998.

[3] Y. Wang, D. Wang, Y. Zhou, J. Zhang, D. Xue, X. Ren, Strain glass as a novel multi-functional material, in: A. Saxena, A. Planes (Eds.), Mesoscopic Phenomena in Multifunctional Materials, vol. 198, Springer Berlin Heidelberg, 2014, pp. 271–288.

[4] X.B. Ren, Y. Wang, Y.M. Zhou, Z. Zhang, D. Wang, G.L. Fan, K. Otsuka, T. Suzuki, Y.C. Ji, J. Zhang, Y. Tian, S. Hou, X.D. Ding, Strain glass in ferroelastic systems: premartensitic tweed versus strain glass, Philos. Mag. 90 (2010) 141–157.

[5] Y. Wang, X.B. Ren, K. Otsuka, Shape memory effect and superelasticity in a strain glass alloy, Phys. Rev. Lett. 97 (2006) 225703.

[6] J. Zhang, Y. Wang, X. Ding, Z. Zhang, Y. Zhou, X. Ren, K. Otsuka, J. Sun, M. Song, Stress-induced strain glass to martensite (R) transition in a $Ti_{50}Ni_{44.5}Fe_{5.5}$ alloy, Phys. Rev. B 83 (2011) 174204.

[7] K. Niitsu, T. Omori, R. Kainuma, Stress-induced transformation behaviors at low temperatures in Ti-51.8Ni (at. %) shape memory alloy, Appl. Phys. Lett. 102 (2013) 231915.

[8] Y. Wang, Y.M. Zhou, J. Zhang, X.D. Ding, S. Yang, X.P. Song, X.B. Ren, K. Otsuka, Evolution of the relaxation spectrum during the strain glass transition of $Ti_{48.5}Ni_{51.5}$ alloy, Acta Mater. 58 (2010) 4723–4729.

[9] Y. Zhou, D. Xue, X. Ding, Y. Wang, J. Zhang, Z. Zhang, D. Wang, K. Otsuka, J. Sun, X. Ren, Strain glass in doped $Ti_{-50}(Ni_{50-x}D_x)$ (D = Co, Cr, Mn) alloys: implication for the generality of strain glass in defect-containing ferroelastic systems, Acta Mater. 58 (2010) 5433–5442.

[10] Z. Zhang, Y. Wang, D. Wang, Y.M. Zhou, K. Otsuka, X.B. Ren, Phase diagram of $Ti_{50-x}Ni_{50+x}$: crossover from martensite to strain glass, Phys. Rev. B 81 (2010) 224102.

[11] D. Wang, Z. Zhang, J. Zhang, Y. Zhou, Y. Wang, X. Ding, Y. Wang, X. Ren, Strain glass in Fe-doped Ti-Ni, Acta Mater. 58 (2010) 6206–6215.

[12] Y. Zhou, D. Xue, X. Ding, K. Otsuka, J. Sun, X. Ren, High temperature strain glass in $Ti_{50}(Pd_{50-x}Cr_x)$ alloy and the associated shape memory effect and superelasticity, Appl. Phys. Lett. 95 (2009).

[13] J. Liu, M. Jin, C. Ni, Y. Shen, G. Fan, Z. Wang, Y. Zhang, C. Li, Z. Liu, X. Jin, Strain glassy behavior and premartensitic transition in $Au_7Cu_5Al_4$ alloy, Phys. Rev. B 84 (2011) 140102.

[14] Y.G. Yao, Z.M. Sun, Y.C. Ji, Y.D. Yang, X.L. Tan, X.B. Ren, Evolution of the tetragonal to rhombohedral transition in (1-x)($Bi_{1/2}Na_{1/2}$)TiO3-xBaTiO$_3$ (x < 7%), Sci. Technol. Adv. Mater. 14 (2013).

[15] J.A. Monroe, J.E. Raymond, X. Xu, M. Nagasako, R. Kainuma, Y.I. Chumlyakov, R. Arroyave, I. Karaman, Multiple ferroic glasses via ordering, Acta Mater. 101 (2015) 107–115.

[16] Y. Wang, C.H. Huang, H.J. Wu, J.H. Gao, S. Yang, D. Wang, X.D. Ding, X.P. Song, X.B. Ren, Spontaneous strain glass to martensite transition in ferromagnetic Ni-Co-Mn-Ga strain glass, Appl. Phys. Lett. 102 (2013).

[17] Y.C. Ji, X.D. Ding, T. Lookman, K. Otsuka, X.B. Ren, Heterogeneities and strain glass behavior: role of nanoscale precipitates in low-temperature-aged $Ti_{48.7}Ni_{51.3}$ alloys, Phys. Rev. B 87 (2013).

[18] Z. Zhou, J. Cui, X. Ren, Strain glass state as the boundary of two phase transitions, Sci. Rep. 5 (2015) 13377.

[19] W. Tirry, D. Schryvers, Linking a completely three-dimensional nanostrain to a structural transformation eigenstrain, Nat. Mater. 8 (2009) 752–757.

[20] D. Wang, Y. Wang, Z. Zhang, X. Ren, Modeling abnormal strain states in ferroelastic systems: the role of point defects, Phys. Rev. Lett. 105 (2010).

[21] K. Otsuka, X. Ren, Physical metallurgy of Ti-Ni-based shape memory alloys, Prog. Mater. Sci. 50 (2005) 511–678.

[22] R. Vasseur, D. Xue, Y. Zhou, W. Ettoumi, X. Ding, X. Ren, T. Lookman, Phase diagram of ferroelastic systems in the presence of disorder: analytical model and experimental verification, Phys. Rev. B 86 (2012).

[23] U. Messerschmidt, Dislocation Dynamics During Plastic Deformation, Springer Berlin Heidelberg, 2010.

[24] J. Zhang, Y. Wang, X. Ding, Z. Zhang, Y. Zhou, X. Ren, D. Wang, Y. Ji, M. Song, K. Otsuka, J. Sun, Spontaneous strain glass to martensite transition in a $Ti_{50}Ni_{44.5}Fe_{5.5}$ strain glass, Phys. Rev. B 84 (2011).

[25] J. Zhang, C. Somsen, T. Simon, X. Ding, S. Hou, S. Ren, X. Ren, G. Eggeler, K. Otsuka, J. Sun, Leaf-like dislocation substructures and the decrease of martensitic start temperatures: a new explanation for functional fatigue during thermally induced martensitic transformations in coarse-grained Ni-rich Ti–Ni shape memory alloys, Acta Mater. 60 (2012) 1999–2006.

[26] M.S. Choi, T. Yamamoto, T. Fukuda, T. Kakeshita, E. Taguchi, H. Mori, [23] Differences between the R-phase and the commensurate phase in iron-doped Ti-Ni shape memory alloys, Philos. Mag. 88 (2008) 2449–2460.

[27] S. Kustov, D. Salas, E. Cesari, R. Santamarta, D. Mari, J. Van Humbeeck, Structural anelasticity, elasticity and broken ergodicity in Ni–Ti shape memory alloys, Acta Mater. 73 (2014) 275–286.

[28] X. Ren, Strain glass and ferroic glass – unusual properties from glassy nanodomains, Phys. Status Solidi (b) 251 (2014) 1982–1992.

[29] G. Burns, F. Dacol, Glassy polarization behavior in ferroelectric compounds $Pb(Mg_{13}Nb_{23})O_3$ and $Pb(Zn_{13}Nb_{23})O_3$, Solid State Commun. 48 (1983) 853–856.

[30] D. Schryvers, S. Cao, S. Pourbabak, H. Shi, J.B. Lu, Recent EM investigations on nano- and micro-defect structures in SMAs, J. Alloys Compd. 577 (Suppl. 1) (2013) S705–S709.

[31] J.K. Allafi, X. Ren, G. Eggeler, The mechanism of multistage martensitic transformations in aged Ni-rich NiTi shape memory alloys, Acta Mater. 50 (2002) 793–803.

[32] J. Khalil-Allafi, A. Dlouhy, G. Eggeler, Ni4Ti3-precipitation during aging of NiTi shape memory alloys and its influence on martensitic phase transformations, Acta Mater 50 (2002) 4255–4274.